

Discovery of Tropifexor (LJN452), a Highly Potent Non-Bile Acid FXR Agonist for the Treatment of Cholestatic Liver Diseases and Nonalcoholic Steatohepatitis (NASH)

David C. Tully, Paul V Rucker, Donatella Chianelli, Jennifer Williams, Agnes Vidal, Phil B. Alper, Daniel Mutnick, Badry Bursulaya, James Schmeits, Xiangdong Wu, Dingjiu Bao, Jocelyn Zoll, Young Kim, Todd Groessl, Peter McNamara, H. Martin Seidel, Valentina Molteni, Bo Liu, Andrew Phimister, Sean B Joseph, and Bryan Laffitte

J. Med. Chem., **Just Accepted Manuscript** • Publication Date (Web): 16 Nov 2017

Downloaded from <http://pubs.acs.org> on November 16, 2017

Just Accepted

“Just Accepted” manuscripts have been peer-reviewed and accepted for publication. They are posted online prior to technical editing, formatting for publication and author proofing. The American Chemical Society provides “Just Accepted” as a free service to the research community to expedite the dissemination of scientific material as soon as possible after acceptance. “Just Accepted” manuscripts appear in full in PDF format accompanied by an HTML abstract. “Just Accepted” manuscripts have been fully peer reviewed, but should not be considered the official version of record. They are accessible to all readers and citable by the Digital Object Identifier (DOI®). “Just Accepted” is an optional service offered to authors. Therefore, the “Just Accepted” Web site may not include all articles that will be published in the journal. After a manuscript is technically edited and formatted, it will be removed from the “Just Accepted” Web site and published as an ASAP article. Note that technical editing may introduce minor changes to the manuscript text and/or graphics which could affect content, and all legal disclaimers and ethical guidelines that apply to the journal pertain. ACS cannot be held responsible for errors or consequences arising from the use of information contained in these “Just Accepted” manuscripts.

1
2
3
4
5
6
7
8
9
10
11
12
13
14
15
16
17
18
19
20
21
22
23
24
25
26
27
28
29
30
31
32
33

Discovery of Tropifexor (LJN452), a Highly Potent Non-Bile Acid FXR Agonist for the Treatment of Cholestatic Liver Diseases and Nonalcoholic Steatohepatitis (NASH)

16 *David C. Tully, *^{†‡} Paul V. Rucker,[†] Donatella Chianelli,[†] Jennifer Williams,[†] Agnès Vidal,[†] Phil B. Alper,[†] Daniel Mutnick,[†] Badry Bursulaya,[†] James Schmeits,[†] Xiangdong Wu,[†] Dingjiu Bao,[†] Jocelyn Zoll,[†] Young Kim,[†] Todd Groessl,[†] Peter McNamara,[†] H. Martin Seidel,^{†◇} Valentina Molteni,[†] Bo Liu,[†] Andrew Phimister,^{‡1} Sean B. Joseph,^{†§} and Bryan Laffitte[†]*

27 [†]Genomics Institute of the Novartis Research Foundation, San Diego, California 92121

30 [‡]Novartis Institutes for Biomedical Research, Emeryville, California 94608

34 **KEYWORDS** Farnesoid X Receptor, FXR Agonist, cholestasis, dyslipidemia, nonalcoholic
35 steatohepatitis (NASH)
36
37
38
39

40 **ABSTRACT:** The farnesoid X receptor (FXR) is a nuclear receptor that acts as a master regulator of
41 bile acid metabolism and signaling. Activation of FXR inhibits bile acid synthesis and increases bile
42 acid conjugation, transport, and excretion, thereby protecting the liver from the harmful effects of bile
43 acid accumulation, leading to considerable interest in FXR as a therapeutic target for the treatment of
44 cholestasis and non-alcoholic steatohepatitis. We identified a novel series of highly potent non-bile acid
45 FXR agonists that introduce a bicyclic nortropine-substituted benzothiazole carboxylic acid moiety onto
46 a trisubstituted isoxazole scaffold. Herein, we report the discovery of 1 (tropifexor, LJN452) a novel
47 and highly potent agonist of FXR. Potent in vivo activity was demonstrated in rodent PD models
48
49
50
51
52
53
54
55
56
57
58
59
60

1 measuring the induction of FXR target genes in various tissues. Tropifexor has advanced into Phase 2
2
3 human clinical trials in patients with NASH and PBC.
4
5
6

7 INTRODUCTION AND BIOLOGICAL RATIONALE

9
10 The farnesoid X receptor (FXR) is a ligand-activated nuclear receptor that is highly expressed
11 in the liver, gall bladder, intestines and kidney, and acts as a key regulator of bile acid
12 production, conjugation, and transport.¹ Bile acids are resorbed in the ileum and activate FXR,
13 which leads to increased expression of bile acid binding proteins and FGF19, a key metabolic
14 regulator. In the liver, FXR activation modulates expression of genes involved in bile acid
15 transport and metabolism, as well as glucose and lipid metabolism. Specifically, activation of
16 FXR directly increases the expression of enzymes responsible for bile acid detoxification and
17 canalicular and basolateral bile acid efflux, while also inhibiting bile acid synthesis and
18 basolateral bile acid uptake by hepatocytes.² Activation of FXR can repress bile acid synthesis
19 by either of two complementary mechanisms. In the liver, FXR activation induces SHP
20 (NR0B2) which is a negative regulator of CYP7A1 expression, an enzyme which catalyzes the
21 rate limiting step of the neutral bile acid biosynthetic pathway.³ Activation of FXR in the
22 intestines induces transcription of the endocrine hormone FGF19, which is secreted into portal
23 circulation and subsequently binds to the FGFR4 receptor in the liver, which in turn activates a
24 MAPK signalling pathway that results in the downregulation of CYP7A1 expression, thereby
25 inhibiting bile acid synthesis.⁴
26
27
28
29
30
31
32
33
34
35
36
37
38
39
40
41
42
43
44
45
46

47 Cholestasis is a pathological condition in which bile flow from the liver to the intestine is
48 reduced or interrupted due either to impaired secretion by hepatocytes, or to obstruction of bile
49 flow through the bile ducts. The consequence of the accumulation of bile salts is disruption of
50 cellular membranes, which results in injury to the affected tissues, whereby the liver is typically
51 most affected. Primary biliary cholangitis (PBC) is a chronic and progressive cholestatic
52
53
54
55
56
57
58
59
60

1
2
3 disease, presumed to be autoimmune in origin, which results from the progressive destruction of
4
5 intrahepatic bile ducts.⁵ Decreased FXR expression and mutations of the FXR target genes
6
7 ABCB11 (encoding BSEP) or ABCB4 (encoding MDR3) are observed in hereditary forms of
8
9 human cholestasis and lead to a severe form of cholestasis known as progressive familial
10
11 intrahepatic cholestasis (PFIC-2 and -3).^{6,7} In addition, loss-of-function mutations in the NR1H4
12
13 gene that encodes FXR have been determined to be the cause for a neonatal form of PFIC.⁸
14
15 Ursodeoxycholic acid (UDCA) is a naturally occurring primary bile acid, and though not an FXR
16
17 agonist, is currently the standard of care for the treatment of PBC. Obeticholic acid (OCA), a
18
19 synthetic bile-acid FXR agonist, recently received accelerated approval for the treatment of PBC
20
21 in combination with UDCA for patients who do not respond adequately to UDCA therapy
22
23 alone.⁹
24
25
26
27
28

29
30 In addition to its role in bile acid metabolism and signaling, FXR is also involved in regulation
31
32 of triglyceride metabolism and lipogenesis. FXR activation suppresses the activity of SREBP-
33
34 1c, a key transcription factor that regulates triglyceride synthesis by inducing enzymes involved
35
36 in lipogenesis. Non-alcoholic steatohepatitis (NASH) is a condition characterized by the
37
38 accumulation of fat in the liver (steatosis), inflammation, hepatocyte ballooning, and fibrosis.
39
40 NASH is a leading cause of cirrhosis and liver transplantation, and cases are expected to rise due
41
42 to the increased prevalence worldwide of obesity and type 2 diabetes. It is hypothesized that
43
44 FXR activation can reduce the liver steatosis, inflammation and fibrosis in patients with NASH
45
46 by suppressing lipogenesis and promoting triglyceride oxidation and clearance.
47
48
49

50
51 In a recent clinical trial in patients with NASH, treatment with OCA led to improvements in
52
53 serum transaminases and liver histology,¹⁰ however, higher rates of pruritus were experienced by
54
55 patients treated with OCA compared to placebo-treated patients.^{10,11} Pruritus, or severe itch, is a
56
57
58
59
60

1
2
3 common symptom associated with cholestatic disorders, and recent clinical trials have
4 demonstrated that OCA therapy in patients with PBC further exacerbates pruritus, which may
5 ultimately limit the clinical utility of OCA in susceptible patient populations.^{11,12} OCA also
6 caused adverse effects on serum lipid profiles including elevated LDL cholesterol and total
7 cholesterol in healthy volunteers and in patients with NASH, which is a concern in a patient
8 population with an elevated risk for cardiovascular disease.¹⁰⁻¹³
9
10
11
12
13
14
15
16

17 Our efforts to discover safe and more effective therapies for the treatment of cholestatic
18 disorders have focused on the development of novel FXR agonists to improve upon the efficacy,
19 safety, and tolerability of the current standard of care. To achieve this goal, the intended target
20 drug candidate profile was for a highly potent and selective, non-bile acid, FXR agonist that
21 would be effective at low systemic exposures. As FXR is expressed predominantly in the liver
22 and intestines, the desire to limit the oral bioavailability and avoid high systemic exposures
23 stemmed from the wish to avoid the prolonged systemic activation of FXR. Herein, we report
24 our discovery of a novel series of highly potent non-bile acid FXR agonists that features a
25 bicyclic [3.2.1] tropane linker ring as the key component responsible for the exceptional potency.
26 This series potently and selectively activates FXR in vitro, and optimized analogs potently
27 regulate FXR target genes in vivo at very low systemic exposures in preclinical
28 pharmacodynamic models. The most advanced compound from this series (**1**) has progressed
29 into Phase II clinical trials for the treatment of patients with PBC¹⁴ and NASH.¹⁵
30
31
32
33
34
35
36
37
38
39
40
41
42
43
44
45
46
47
48

49 **BACKGROUND**

50
51 Researchers at Glaxo-SmithKline (GSK) previously described the biological and
52 pharmacological activity of the synthetic FXR agonist GW4064 (**2**).¹⁶ Since this initial report,
53 there have been extensive optimization efforts by several groups to overcome liabilities of this
54
55
56
57
58
59
60

1
2
3 scaffold class such as low aqueous solubility and overall poor ADME and PK properties.¹⁷⁻²²
4
5 Detailed accounts of much of this research has been thoroughly summarized in recent review
6
7 articles.^{23,24} Researchers at GSK demonstrated that the stilbene moiety of **2** could be replaced
8
9 with a fused biaryl ring system such as the isoquinoline in GSK2324 (**3**, EC₅₀ = 50 nM, 102%
10
11 efficacy).¹⁸ This additional conformational restraint retained potent in vitro activity with full
12
13 efficacy; however such analogs likely lacked the necessary physicochemical properties and PK
14
15 to progress into development. More recently, researchers at Eli Lilly reported that the central
16
17 phenyl ring could be replaced by a piperidine ring exemplified by **4** (LY2562175, EC₅₀ = 193
18
19 nM, 41% efficacy).²⁵ The replacement of the extended conjugated aromatic system with a
20
21 piperidine linker resulted in an improvement in overall drug-like properties, despite resulting in a
22
23 loss of potency and only partial FXR agonist activity relative to **2** and **3**.
24
25
26
27
28
29

30 RESULTS AND DISCUSSION

31
32 Early in our efforts to identify a novel full FXR agonist with improved potency and PK, we
33
34 discovered that replacement of the indole moiety of the partial FXR agonist **4** with a 2-
35
36 substituted benzothiazole-6-carboxylic acid resulted in a dramatic improvement in potency and
37
38 exhibited full agonist efficacy in a cellular assay.^{26,27} The ligand-induced interaction with a
39
40 coactivator protein is a critical step in transcriptional activation by FXR, and this is determined
41
42 in the FXR-HTRF biochemical assay that measures the interaction between FXR and the Steroid
43
44 Receptor Coactivator-1 (SRC1). Benzothiazole **5** was determined to have an EC₅₀ = 8.3 nM with
45
46 96% efficacy relative to **2**, the most commonly used comparator FXR agonist (Table 1). The
47
48 potent functional activity of **5** translates well in the FXR BSEP-luc reporter gene cellular assay,
49
50 which is designed to measure cellular transcriptional activity of full length FXR on the BSEP
51
52
53
54
55
56
57
58
59
60

1
2
3 promoter driving a luciferase reporter gene. Compound **5** has an $EC_{50} = 9.5$ nM in this cellular
4
5 assay and activates FXR as a full agonist with 118% efficacy relative to **2**.
6
7

8 The pharmacokinetics in rats was determined, and **5** exhibited high plasma clearance and low
9
10 oral bioavailability ($F = 6\%$) (Table 2). In vitro metabolic stability in rat and human liver
11
12 microsomes (RLM, HLM) showed moderate to high extraction ratios, (Table 1) which was
13
14 consistent with the observed in vivo rat clearance, and suggested that oral bioavailability was
15
16 limited by the high in vivo clearance. Furthermore, in vitro metabolite ID studies in liver
17
18 microsomes suggested oxidative metabolism on the 2,6-dichlorophenyl ring as the primary route
19
20 for metabolic clearance, which was not surprising due to the highly lipophilic nature of that
21
22 moiety.
23
24
25

26
27 Having identified that benzothiazole moiety provides a significant improvement in potency
28
29 versus **4** with full agonist efficacy, this carboxylic acid-bearing pharmacophore was fixed while
30
31 exploring the SAR in other regions of the scaffold for further optimization. In order to reduce
32
33 address the metabolic liability, replacement of the 2,6-dichlorophenyl group was explored in the
34
35 attempt to improve the metabolic clearance and aqueous solubility. Replacement of the 2,6-
36
37 dichlorophenyl with either 2,6-difluorophenyl (**6**) or 2-trifluoromethylphenyl (**7**) resulted in a
38
39 modest loss of FXR agonist activity, and metabolic stability in RLM was not improved, although
40
41 the HLM stability showed some improvement compared to **5**. In contrast, the 2-
42
43 trifluoromethoxyphenyl group (compound **8**) proved to be highly beneficial in several respects.
44
45 Compound **8**, in addition to improved FXR agonist activity ($EC_{50} = 19$ nM) and full efficacy
46
47 (100%), showed a notable improvement in metabolic stability, with low extraction ratios in rat
48
49 and human liver microsomes. The improvement in the in vitro metabolic stability translated
50
51
52
53
54
55
56
57
58
59
60

1
2
3 nicely in vivo, as **8** had significantly improved rat pharmacokinetics versus the 2,6-dichloro
4 analog **5**, with moderate clearance (24 mL/min/kg) and modest oral bioavailability (F = 37%).
5
6

7
8 Next, we examined the SAR involving replacements for the piperidine ring which serves as the
9 framework linking the essential trisubstituted isoxazole pharmacophore to the aryl carboxylic
10 acid moiety. A decrease in ring size to the azetidine (**9**) or pyrrolidine (**10**) was not tolerated,
11 and resulted in a substantial loss of FXR agonist activity (>100-fold). Conversely, an increase in
12 ring size to the racemic azepane (**11**) afforded a modest improvement in potency compared to
13 piperidine **8**. However, despite this improvement in FXR potency versus the piperidine **8**, the
14 azepane analog **11** was undesirable due to its poor metabolic stability in liver microsomes, and
15 displayed high extraction ratios in both RLM and HLM (0.75, 0.89).
16
17
18
19
20
21
22
23
24
25
26

27 In the continued effort to optimize the linker moiety, we sought to increase the conformational
28 restraint of this central scaffolding ring. We therefore installed the 8-azabicyclo[3.2.1]octane ring
29 derived from nortropine, which resulted in a dramatic improvement in potency. Nortropine **12**
30 had full FXR agonist efficacy with sub-nM potency in both the FXR-HTRF coactivator
31 interaction assay (EC₅₀ = 0.54 nM) and FXR BSEP-luc cellular assay (EC₅₀ = 0.69 nM). This
32 significant development represented a 30-fold improvement in potency over piperidine precursor
33 **8**, and more than two orders of magnitude greater potency versus **4**.
34
35
36
37
38
39
40
41
42

43 Importantly, the in vitro ADME properties of nortropine **12** were attractive, with decent
44 solubility (110 μM) in fasted state simulated intestinal fluid (FASSIF, pH = 6.8), and it showed
45 moderate and low extraction ratios in rat (0.51) and human (<0.20) liver microsomes,
46 respectively. Nortropine **12** exhibited reduced plasma clearance in rats (CL = 17 mL/min/kg)
47 versus piperidine **8**, although the terminal half-life was short and oral bioavailability was low (F
48 = 11%) (Table 2). Having achieved a remarkable improvement in potency for this scaffold, we
49
50
51
52
53
54
55
56
57
58
59
60

1
2
3 focused on further optimization of this promising nortropine lead. The focus of continued
4 optimization remained to achieve reduced metabolic clearance and longer in vivo half-life in
5 order to improve in vivo activity in a rodent PD model measuring induction of FXR target genes
6 in the liver and intestines. Along with preserving the highly potent FXR agonist activity, limited
7 systemic exposure and oral bioavailability was desired in order to minimize prolonged systemic
8 activation in FXR, particularly in tissues other than liver and intestines.
9

10
11 To this end, we examined the influence of various substituents at the synthetically accessible
12 4-position of the benzothiazole ring (Table 3). While the addition of either a methyl (**13**) or
13 methoxy (**14**) group retained potent FXR activity, the rat PK was not significantly improved, as
14 both compounds had low oral bioavailability and short $T_{1/2}$, despite the low clearance (Table 2).
15
16 In contrast, the 4-fluoro substituted analog **1** gave further modest improvement in the FXR
17 agonist activity ($EC_{50} = 0.26$ nM) compared to **12** with full agonist activity in the FXR BSEP
18 cellular assay. Likewise the solubility in FASSIF (600 μ M) was improved considerably
19 compared to close analogs **12**, **13**, and **14**, possibly explained by the lower pKa of the 4-fluoro
20 substituted benzothiazole carboxylic acid (pKa = 4.0).
21
22

23
24 Moreover, the rat pharmacokinetics were further improved, as compound **1** had low clearance
25 (CL = 9 mL/min/kg) and a significantly longer terminal half-life ($T_{1/2} = 3.7$ h) than what had
26 been observed with previous analogs from this scaffold, and was consistent with the low
27 extraction ratio seen in rat liver microsomes. Oral bioavailability of **1** in the rat was 20% from
28 an aqueous microemulsion formulation, a modest improvement over other nortropine analogs
29 (Table 2). With the 4-fluorobenzothiazole in place, further examination of the phenyl ring
30 substituent demonstrated that the ortho-trifluoromethoxy group could be modified to either
31
32
33
34
35
36
37
38
39
40
41
42
43
44
45
46
47
48
49
50
51
52
53
54
55
56
57
58
59
60

1
2
3 difluoromethoxy **15** or trifluoromethyl **16** (LJP305) while preserving similarly potent FXR
4
5 agonist activity with comparable rat pharmacokinetics.
6
7

8 To help rationalize the remarkable boost in potency attained through the introduction of the
9
10 novel nortropine-benzothiazole pharmacophore, we examined computational molecular
11
12 modeling simulations of **1** docked into the X-ray structure of the FXR ligand binding domain
13
14 (PDB 3DCT). In good agreement with published X-ray co-crystal structures of related
15
16 isoxazoles bound to the FXR ligand binding domain, the docking model in Figure 2 showed the
17
18 key H-bond between the isoxazole nitrogen and H447 and hydrophobic interactions with W468
19
20 of helix 12.¹⁷⁻¹⁹ The cyclopropyl group fills the hydrophobic pocket formed by side chains of
21
22 F284, L287, F461, and W454, while the 2-trifluoromethoxyphenyl ring establishes hydrophobic
23
24 contacts with M328, M365, and I352. The bridged bicyclic nortropine ring system fills the
25
26 central portion of the binding pocket, and, due to its limited flexibility, provides conformational
27
28 restraint to the central linker section of the ligand. Furthermore, the ethylene bridge establishes a
29
30 favorable intramolecular hydrophobic interaction with the face of the 2-trifluoromethoxyphenyl
31
32 ring. Additionally, the benzothiazole ring efficiently fills the narrow portion of the hydrophobic
33
34 pocket and delivers the optimal geometry for the carboxylic acid substituent to establish the
35
36 essential electrostatic interaction with R331 in helix 5.
37
38
39
40
41
42

43 Having achieved the optimization of highly potent FXR agonists with improved rat PK,
44
45 compounds **1** and **16** were selected for further evaluation in pre-clinical models of FXR
46
47 activation. Compound **1** was examined in rat primary hepatocytes in an assay designed to
48
49 measure the induction of FXR target genes BSEP and SHP mRNA by quantitative real-time PCR
50
51 (qPCR). Robust induction of both target genes was observed in primary cells by **1** in a
52
53 concentration-dependent manner (Figure 3). BSEP induction above vehicle (DMSO) control
54
55
56
57
58
59
60

1
2
3 was observed at concentrations as low as 1 nM, while strong induction of SHP (15-fold above
4 vehicle) was observed at 10 nM, and modest induction of SHP at 1 nM (3-fold).
5
6

7
8 Compounds **1** and **16** were evaluated in a PD model designed to measure the induction of FXR
9 target genes in the rat following a single oral dose. Both test compounds were administered
10 orally using a range of four doses (0.03, 0.1, 0.3, and 1.0 mg/kg) and compared directly to the
11 vehicle control group (vehicle: 0.5% methylcellulose, 0.5% Tween80, 99% water, suspension).
12
13 Tissues were harvested 7 h post-dose, and mRNA was isolated from the liver and ileum and
14 analyzed by real-time quantitative PCR using primer and probe sets specific to SHP (NR0B4),
15 BSEP (ABCB11) and FGF15. Both compounds demonstrated robust induction of FXR target
16 genes in a dose-dependent fashion with highly potent in vivo activity. Similar levels of induction
17 of SHP in the liver were observed, with maximal induction of ~6-fold achieved at 1.0 mg/kg for
18 both compounds **1** and **16**, while significant BSEP induction was observed at the lower dose of
19 0.3 mg/kg (Figure 4). In the ileum, where FXR is also highly expressed, FXR target genes SHP
20 and FGF15 (rodent ortholog of human FGF19) were potently induced by **16** at 0.3 mg/kg (Figure
21 4). Even more impressively, compound **1** demonstrated highly potent induction of SHP and
22 FGF15 in the ileum as doses as low as 0.1 mg/kg, with mRNA levels >20-fold above vehicle
23 treated animals (Figure 5).
24
25
26
27
28
29
30
31
32
33
34
35
36
37
38
39
40
41
42

43 In order to more extensively evaluate the pharmacological activity and PK/PD relationship of
44 compound **1** at steady state, an integrated PK/PD study was carried out in naïve rats that were
45 treated orally with compound **1** once daily for 14 days. Considering the potent activity observed
46 in the previous single dose PD study, a wider range of six doses were chosen to better determine
47 the minimally efficacious dose and exposure required for regulation of FXR target genes: 0.003,
48 0.01, 0.03, 0.1, 0.3, 1.0, and 3.0 mg/kg, all administered orally using a standard suspension
49
50
51
52
53
54
55
56
57
58
59
60

1
2
3 formulation (0.5% methylcellulose, 0.5% Tween80, 99% water). Multiple plasma samples were
4
5 collected from each group on days 1 and 11 for determination of pharmacokinetics. Tissues
6
7 (liver and ileum) were harvested on day 14 of the study 7 h after the final dose, and mRNA was
8
9 analyzed by real-time qPCR. In addition, the total compound concentrations in the liver were
10
11 determined at 1 h and 7 h for each dosing group.
12
13
14

15 In the liver, robust induction of SHP was observed at 0.01 mg/kg of compound **1** with maximal
16
17 levels of gene induction achieved at 0.3 mg/kg. Initial BSEP induction in the liver appeared at
18
19 the lowest dose tested (0.003 mg/kg), and maximal BSEP target gene induction was achieved
20
21 above 0.1 mg/kg (Figure 6). Activation of FXR in the liver resulted in the downregulation of
22
23 sterol 12- α hydroxylase (CYP8B1) gene transcription, thereby reducing the conversion of
24
25 cholesterol to bile acids. Expression of CYP8B1 mRNA following 14 day treatment with **1** was
26
27 already apparent at the lowest dose (0.003 mg/kg), and CYP8B1 gene expression was fully
28
29 repressed at doses above 0.03 mg/kg. Extrapolation of the data provided a mean ED₅₀ of
30
31 approximately 0.02 mg/kg in the liver for SHP and BSEP and 0.01 mg/kg for CYP8B1 (Table 4).
32
33 In the ileum, FXR target genes SHP and FGF15 are robustly induced at similarly low doses
34
35 down to 0.01 mg/kg as shown in Figure 7. The mean ED₅₀ for induction of SHP in the ileum
36
37 was determined to be approximately 0.01 mg/kg, while for FGF15 in the ileum ED₅₀ was around
38
39 0.05 mg/kg.
40
41
42
43
44
45

46 Serum triglycerides and plasma FGF15 protein levels were also analyzed, as these circulating
47
48 biomarkers could potentially be utilized as clinically translatable indicators of target engagement.
49
50 Activation of FXR in the ileum induces the expression of FGF15/FGF19, which is then secreted
51
52 in the portal blood and signals repression of CYP7A1 expression in the liver. In agreement with
53
54 the observation of increased FGF15 mRNA expression in the ileum, treatment of rats with
55
56
57
58
59
60

1
2
3
4
5
6
7
8
9
10
11
12
13
14
15
16
17
18
19
20
21
22
23
24
25
26
27
28
29
30
31
32
33
34
35
36
37
38
39
40
41
42
43
44
45
46
47
48
49
50
51
52
53
54
55
56
57
58
59
60

compound **1** exhibited a clear dose-dependent increase in plasma FGF15 protein, with maximal levels of FGF15 detected at 7 h post-dose (Figure 8). Importantly, at 24 h following the final dose, plasma FGF15 protein concentrations had normalized to baseline levels, suggesting that repeat daily administration of compound **1** does not result in the prolonged activation of FXR.

Serum triglycerides are an indirect biomarker of FXR activation, whereby FXR directly induces SHP and downregulates the transcription factor SREBP-1c which is a master regulator of fatty acid and lipid synthesis. Treatment with compound **1** for 14 days produced a robust dose-dependent reduction in serum triglycerides and reached a maximal response with a 0.3 mg/kg dose, resulting in a decrease of triglyceride levels to approximately 79% below the vehicle control group (Figure 9).

Plasma samples were collected at multiple time points (0.5, 1, 3, 7, and 24 h) on days 1 and 11 for determination of the pharmacokinetics of compound **1** in this study following the first dose and at steady state. The plasma C_{max} occurred between 3 h and 7 h, and total concentrations were generally similar on day 1 as on 11, ranging from 150 pM at the lowest dose to 171 nM at the highest dose. Compound **1** demonstrated a linear increase in exposure with increasing dose across the entire range of doses. The plasma exposures were very low at efficacious doses, with AUC ranging from 2 nM*h at the lowest dose (0.003 mg/kg) up to 1688 nM*h at the highest dose (3.0 mg/kg) (Table 5 and Figure 10). Importantly, no significant accumulation was observed at steady state following multiple days of administration compared to the exposures observed on day 1 following the initial dose.

Liver exposures were determined at the end of study on day 14 at 1 h and 7 h following the final dose (Table 6). Mean concentrations of **1** in the liver were low single digit nM levels at the lowest doses, and ranged between 600-900 nM at the highest dose. The liver concentrations

1
2
3 averaged approximately 9-fold higher than mean plasma concentrations, with the exception of
4
5 the two lowest doses, which showed somewhat higher liver:plasma concentration ratios (average
6
7 of 18.5). The higher liver:plasma ratios observed at the two lowest doses may have been due to
8
9 inherent variability in the quantitation methods as the plasma concentrations were well below 1
10
11 nM and near the limit of detection.
12
13

14
15 It is noteworthy that efficacy was observed at such low doses (mean ED₅₀ range 0.01–0.05
16
17 mg/kg) with plasma C_{max} concentrations near 1 nM and below, especially considering that PPB
18
19 of compound **1** is approximately 99.9%. This implies that the unbound concentration of **1** in the
20
21 plasma is well below the cellular EC₅₀ (0.26 nM) at efficacious doses. Moreover, the minimal
22
23 total plasma concentrations of **1** that are sufficient to regulate FXR target gene expression in the
24
25 liver and intestines are only marginally higher than the cellular EC₅₀ (day 11 C_{max} = 1.9 at 0.03
26
27 mg/kg dose). The liver concentrations of **1** at the lowest effective doses (0.01 and 0.03 mg/kg,
28
29 nearest to ED₅₀ values in Table 4) ranged from 5 nM to 12 nM, which are roughly 8 to 22-fold
30
31 higher than corresponding plasma concentrations at the same doses. Unbound concentrations of
32
33 **1** in the liver were not determined in this study since drug concentrations were quantified from
34
35 tissue homogenates, and therefore a strict PK/PD relationship for the free drug concentrations of
36
37 **1** required to regulate target gene expression in tissues cannot be explicitly determined.
38
39 Moreover, while this PK data suggests that the concentration of compound **1** required for
40
41 pharmacological activity is within the vicinity of the cellular EC₅₀, further studies are warranted
42
43 to delineate whether the pharmacodynamics of an FXR agonist regulating target gene expression
44
45 is driven primarily by C_{max} or by AUC.
46
47
48
49
50
51

52
53 It is instructive to compare the minimum effective concentrations of **1** required for induction of
54
55 BSEP and SHP in the liver in the rat PD model to the concentrations required in primary rat
56
57
58
59
60

1
2
3 hepatocytes (Figure 3). The liver concentrations of **1** (5–12 nM) at the lowest effective doses
4
5 (0.01–0.03 mg/kg) are consistent with and in the same range as the lowest effective
6
7 concentrations required in vitro to drive expression of FXR target genes BSEP and SHP in
8
9 primary hepatocytes (1–10 nM range, Figure 3). Considering these relatively low total drug
10
11 concentrations in the liver and very high PPB (~99.9%), it is reasonable to estimate that the
12
13 efficacious free drug concentrations in the liver are likely near or possibly even below the
14
15 cellular EC₅₀ (0.26 nM). This suggests the notion that the activation, or occupancy, of only a
16
17 fraction of the total available receptors is required for a full agonist of FXR to elicit a
18
19 pharmacological response, as is often the case for agonists of other nuclear receptors and
20
21 GPCRs.
22
23
24
25
26

27 Extensive preclinical profiling demonstrated that **1** was highly selective for FXR: a broad
28
29 panel screen of enzyme, ion channel, nuclear receptor, and GPCR assays showed no significant
30
31 off-target activity (>10000-fold selectivity for FXR, data not shown). Importantly, compound **1**
32
33 displayed no measurable activity on TGR5, the bile acid-activated GPCR (>10 μM) (Table 7).
34
35 This is significant as several recent reports have proposed that activation of TGR5 may be
36
37 responsible for mediating bile acid-induced itch.^{28,29} Recent clinical trials in patients with PBC
38
39 treated with OCA have established a dose-dependent relationship between OCA and the
40
41 incidence and severity of pruritus.^{11,30} To further highlight the potential advantages of a non-
42
43 bile acid derived FXR agonist, we also tested OCA and its primary active metabolites, the
44
45 glycine and taurine conjugates of OCA in the same assay measuring TGR5 activation. Whereas
46
47 OCA itself is a rather weak agonist of hTGR5 with EC₅₀ = 0.918 μM (83% efficacy), the glycine
48
49 and taurine conjugates are considerably more potent hTGR5 agonists, with EC₅₀ values 0.315
50
51 μM and 0.205 μM respectively, both with full (100%) efficacy versus control (Table 7).
52
53
54
55
56
57
58
59
60

1
2
3 Following daily administration of OCA, the glycine and taurine conjugates of OCA undergo
4 enterohepatic recirculation and eventually incorporate into the bile acid pool, reaching steady
5 state serum concentrations of 13.8 and 12.3-fold higher than parent OCA itself.³¹ Moreover, at
6 therapeutic doses of OCA, the total concentration of OCA and its taurine and glycine conjugates
7 are near or above the EC₅₀ concentrations for hTGR5 activation, which could help explain the
8 dose-dependent relationship between OCA and pruritus.¹¹
9
10
11
12
13
14
15
16

17 The pharmacokinetics of compound **1** was evaluated in the mouse and in the dog, and this data
18 is shown in Table 8 for comparison to rat PK. In the mouse, following IV administration
19 compound **1** exhibited low clearance and small volume of distribution, similar to the rat, with a
20 half-life of 2.6 h. In the dog, following IV injection, the clearance was low and T_{1/2} was 7.4 h,
21 also with a small volume of distribution (0.46 L/kg). Plasma samples from the dog PK studies
22 were also monitored for any conjugated metabolites of compound **1**. Only very low levels of the
23 acylglucuronide metabolite (≤ 1 nM) could be detected in some animals, however there were no
24 taurine or glycine conjugated metabolites of **1** observed in any of the animals. Oral
25 bioavailability in all three species (mouse, rat, and dog) was about 10% following administration
26 using an aqueous methylcellulose suspension formulation. The pharmacokinetic parameters
27 from all three species were used for prediction of human PK and estimation of the efficacious
28 human clinical dose using GastroPlus modeling and simulation software. Simulated human PK
29 predicted human clearance to be low, with a moderate T_{1/2}, and oral bioavailability projected at
30 17%. Using the simulated human PK, the clinically efficacious human dose of compound **1** was
31 projected to be in the range of 30 μ g to 110 μ g once daily, and thereby supported advancement
32 to the clinic.
33
34
35
36
37
38
39
40
41
42
43
44
45
46
47
48
49
50
51
52
53
54
55
56
57
58
59
60

1
2
3 A first-in-human Phase 1 clinical study was recently completed in which the safety,
4 tolerability, PK, and PD of compound **1** was assessed in healthy volunteers. Compound **1** was
5 found to be generally safe and well-tolerated following single oral doses ranging from 10 μ g to 3
6 mg. Notably, dose-dependent, transient increases in circulating levels of FGF19 protein were
7 observed, demonstrating potent on-target FXR agonist activity. Preliminary data from this
8 clinical study has recently been disclosed,^{32a} and detailed data and results will be published
9 elsewhere.^{32b}
10
11
12
13
14
15
16
17
18
19

20 CHEMICAL SYNTHESIS OF COMPOUND **1**

21
22 The synthesis of compound **1**, outlined in Scheme 1, was initiated from the commercially
23 available 2-(trifluoromethoxy)benzaldehyde (**17a**). Chloroxime **19a** was prepared from aldehyde
24 **17a** by condensation with hydroxylamine, followed by chlorination with NCS, with both steps
25 proceeding in high yield. Next, cycloaddition of **19a** with methyl 3-cyclopropyl-3-
26 oxopropanoate afforded the desired isoxazole **20a** in moderate yield. The methyl ester was then
27 reduced using LiAlH₄ to give the corresponding primary alcohol **21a**. Subsequent bromination
28 of alcohol **21a**, followed by alkylation with N-Boc nortropine under basic conditions resulted in
29 the Boc-protected intermediate **1f**, which was then treated with TFA to afford nortropine **1g**.
30 Benzothiazole **25a** was prepared in two steps from commercially available aniline **23a** which
31 was treated with NaSCN and bromine using the classical Hegerschoff reaction to generate the
32 aminobenzothiazole **24a**. Next, the aminobenzothiazole **24a** was brominated under modified
33 Sandmeyer reaction conditions using *tert*-butyl nitrite to yield the desired bromobenzothiazole
34 **25a**. N-arylation of amine **1g** with **25a** was carried out under mild thermal conditions using
35 Cs₂CO₃ in DMF. Finally, saponification of the methyl ester generated the carboxylic acid **1** in
36
37
38
39
40
41
42
43
44
45
46
47
48
49
50
51
52
53
54
55
56
57
58
59
60

1
2
3 nine total linear steps. The synthesis and characterization of all other analogs is described in
4
5 supporting information and in references 24 and 25.
6
7

8 9 **CONCLUSION**

10
11 Lead optimization successfully overcame the ADME and physicochemical liabilities of earlier
12 phenylisoxazole FXR agonists by significantly improving the potency and modestly improving
13 the ADME and PK properties. Compound **1** is a highly potent and efficacious non-bile acid
14 FXR agonist that is effective at inducing FXR target genes in the liver and intestines following
15 very low doses and systemic exposures. Compound **1** (LJN452, tropifexor) was found to be
16 generally safe and well-tolerated at pharmacologically active doses in healthy volunteers and has
17 progressed into clinical development where it is currently under evaluation in several Phase 2
18 human clinical trials in patients with PBC and NASH.^{14,15}
19
20
21
22
23
24
25
26
27
28
29

30 31 **EXPERIMENTAL SECTION**

32 33 **Materials and Methods**

34
35 Commercially available starting materials were used as supplied without further purification.
36
37 Reactions were carried out using dry organic solvents (DCM, ACN, DMF, etc.) unless otherwise
38 noted. Reactions were monitored using thin layer chromatography and an Agilent Technologies
39 1200 series 6140 Quadrupole LC-MS with UV detection at 254 nm in electrospray ionization
40 (ESI) mode. For LC-MS, all retention times reported are at 254 nm UV channel unless
41 otherwise noted. All NMR spectra were recorded on a Bruker AVANCE-400 spectrometer
42 operating at a frequency of 400.13 MHz for ¹H and 100.61 MHz for ¹³C equipped with a 5mm
43 QNP cryoprobe with Z-gradient. Chemical shifts for ¹H and ¹³C spectra were referenced to
44 residual solvent. MS were obtained on an Agilent Technologies 1200 series 6140 Quadrupole
45 LC-MS in electrospray ionization (ESI) mode. HRMS-ESI data were recorded using an Agilent
46
47
48
49
50
51
52
53
54
55
56
57
58
59
60

6520 Accurate-Mass Q-TOF LC-MS system with HPLC-Chip Cube interface and an Agilent 1200 HPLC. All final compounds were isolated analytically pure, >99% purity by HPLC unless otherwise indicated. More information is in the Supporting Information.

N-hydroxy-2-(trifluoromethoxy)benzimidoyl chloride (19a). To a solution of sodium hydroxide (7.00 g, 175 mmol, 1.19 equiv) in water (120 mL) was added a stirred solution of $\text{NH}_2\text{OH}\cdot\text{HCl}$ (11.8 g, 170 mmol, 1.15 equiv) in water (120 mL) at 0 °C. The resulting solution was stirred for 10 min at 0 °C. A solution of 2-(trifluoromethoxy)benzaldehyde **17a** (28.0 g, 147 mmol, 1.00 equiv) in ethanol (120 mL) was then added. The reaction was allowed to stir for an additional 1 h at room temperature, at which point it was diluted with water (500 mL). The aqueous layer was extracted with ethyl acetate (2×700 mL), and the organic layers were combined, washed with brine (2×300 mL), dried over anhydrous sodium sulfate, and concentrated under vacuum to give 30.0 g of (E)-2-(trifluoromethoxy)benzaldehyde oxime **18a** (83% yield). The oxime **18a** was carried directly into the next step without further purification. LC-MS m/z 206.0 (M+H); method A; RT = 1.43 min. NCS (22.0 g, 166 mmol, 1.12 equiv) was slowly added to a stirred solution of (E)-2-(trifluoromethoxy) benzaldehyde oxime **18a** (30.0 g, 146 mmol, 1.00 equiv) in DMF (300 mL) keeping the internal temperature below 25 °C. The reaction mixture was stirred for 1 h at room temperature, and then diluted with water (300 mL) and extracted with ethyl acetate (2×500 mL). The organic layers were combined, washed with brine (5×300 mL), dried over anhydrous sodium sulfate, and concentrated under vacuum to give 35.0 g of N-hydroxy-2-(trifluoromethoxy)benzimidoyl chloride **19a** as a light yellow residue (99% yield). This material was used directly in the next step without further purification. ^1H NMR (d_4 -MeOD, 400 MHz) δ 7.95 – 7.90 (m, 1H), 7.83 (d, J = 7.6, 1H), 7.62– 7.43 (m, 2H). LC-MS m/z 240.0 (M+H); method A; RT = 2.03 min.

Methyl 5-cyclopropyl-3-(2-(trifluoromethoxy)phenyl)isoxazole-4-carboxylate (20a).

Potassium carbonate (11.0 g, 79.7 mmol, 1.09 equiv) was suspended in THF (100 mL), and the mixture was cooled to $-10\text{ }^{\circ}\text{C}$ and treated with a solution of methyl 3-cyclopropyl-3-oxopropanoate (11.0 g, 77.5 mmol, 1.06 equiv) in THF (50 mL) dropwise over 5 minutes. To this reaction mixture was then added a solution of N-hydroxy-2-(trifluoromethoxy)benzimidoyl chloride **19a** (17.6 g, 73.6 mmol, 1.0 equiv) in THF (50 mL) and monitored to ensure that the internal temperature did not exceed $-5\text{ }^{\circ}\text{C}$ during the time of the addition. Following this addition, the reaction was warmed to $35\text{ }^{\circ}\text{C}$. Upon cooling, the reaction mixture was diluted with water (200 mL) and extracted with ethyl acetate (2×300 mL). The organic layer was washed with brine (2×200 mL), dried over anhydrous sodium sulfate, concentrated under vacuum, and then purified by silica gel column chromatography using ethyl acetate/petroleum ether (1:100-1:20) to afford methyl 5-cyclopropyl-3-(2-(trifluoromethoxy)phenyl)isoxazole-4-carboxylate **20a** as a white solid, 12.5 g (52% yield), M.P. $145\text{--}150\text{ }^{\circ}\text{C}$ (broad). ^1H NMR (d_4 -MeOD, 400 MHz) δ 7.65–7.60 (m, 1H), 7.53 (dd, $J = 7.6, 2\text{ Hz}$, 1H), 7.48–7.43 (m, 2H), 3.68 (s, 3H), 2.89 (pentet, $J = 6.8\text{ Hz}$, 1H), 1.30 (app br d, $J = 6.8\text{ Hz}$, 4H). LC-MS m/z 328.1 (M+H); method A; RT = 2.91 min.

(5-Cyclopropyl-3-(2-(trifluoromethoxy)phenyl)isoxazol-4-yl)-methanol (21a). A 250-mL round-bottom flask was purged and maintained with an inert atmosphere of nitrogen, and then charged with a suspension of LiAlH_4 (2.50 g, 65.8 mmol, 2.87 equiv) in THF (50 mL). A solution of methyl 5-cyclopropyl-3-(2-(trifluoromethoxy)phenyl) isoxazole-4-carboxylate **20a** (7.50 g, 22.9 mmol, 1.00 equiv) in tetrahydrofuran (50 mL) was added dropwise at $-10\text{ }^{\circ}\text{C}$. The resulting solution was stirred for 30 min at $-10\text{ }^{\circ}\text{C}$, and the reaction was quenched by the sequential addition of ethyl acetate (3 mL), water (3 mL), and 15% aqueous NaOH (10 mL).

1
2
3 The resulting mixture was filtered through celite, and the filter cake was washed with ethyl
4 acetate (200 mL). The filtrate was washed with brine (2×100 mL), dried over anhydrous sodium
5 sulfate, and concentrated under vacuum, affording 7 g of (5-cyclopropyl-3-(2-
6 (trifluoromethoxy)phenyl)isoxazol-4-yl)methanol **21a** as yellow oil, (93% yield). ¹H NMR
7 (CDCl₃, 400 MHz) δ 7.57–7.55 (m, 2H), 7.41–7.40 (m, 2H), 4.50 (s, 2H), 2.22–2.20 (m, 1H),
8 1.72 (s, 1H) 1.11–1.28 (m, 4H). LC-MS *m/z* 300.1 (M+H); method B; RT = 1.69 min.

9
10
11
12
13
14
15
16
17 **Tert-Butyl 3-((5-cyclopropyl-3-(2-(trifluoromethoxy)phenyl)isoxazol-4-yl)methoxy)-8-**
18 **azabicyclo[3.2.1]octane-8-carboxylate (1f).** Into a 100 mL round bottom flask was placed (5-
19 cyclopropyl-3-(2-(trifluoromethoxy)phenyl)isoxazol-4-yl)-methanol **21a** (4.00 g, 13.3 mmol),
20 triphenylphosphine (5.6 g, 20 mmol, 1.5 equiv), and dichloromethane (40 mL). The mixture was
21 stirred until completely dissolved and then slowly added dropwise to a solution of carbon
22 tetrabromide (6.6 g, 20 mmol, 1.5 equiv) in dichloromethane (20 ml). The reaction was stirred
23 for 1 h, and the solvent was evaporated *in vacuo*. The crude material was purified by silica gel
24 chromatography using a gradient of ethyl acetate/hexanes (0–50%). The bromide **22a** was
25 obtained as a clear oil (4.18 g, 87% yield) and then used immediately (owing to stability) in the
26 next step. ¹H NMR (CDCl₃, 400 MHz) δ 7.55–7.50 (m, 1H), 7.49–7.45 (m, 1H), 7.40–7.32 (m,
27 2H), 4.27 (s, 2H), 2.11–1.99 (m, 1H), 1.24–1.17 (m, 2H), 1.17–1.09 (m, 2H). LC-MS *m/z*
28 362.0/364.0 (M + H); (Br isotope pattern); method B; RT = 1.62 min. Into a dry 250-mL flask
29 was placed N-Boc nortropine (2.9 g, 13 mmol), 18-crown-6 (3.4 g, 12 mmol) and anhydrous
30 THF (80 mL). Potassium *tert*-butoxide (2.9 g, 26 mmol) was added portionwise, and the mixture
31 was stirred vigorously under nitrogen for 1h. 4-(Bromomethyl)-5-cyclopropyl-3-(2-
32 (trifluoromethoxy)-phenyl)isoxazole **22a** (4.18 g, 11.6 mmol) was dissolved in anhydrous THF
33 (20 mL) and added dropwise. The reaction mixture was stirred overnight under a positive
34
35
36
37
38
39
40
41
42
43
44
45
46
47
48
49
50
51
52
53
54
55
56
57
58
59
60

1
2
3 nitrogen pressure. The solvent was removed *in vacuo*, and the mixture was diluted with water
4 (100 mL) and ethyl acetate (100 mL). The organic layer was separated, dried (MgSO₄),
5
6 evaporated under vacuum, and then purified by silica gel chromatography using a gradient of
7
8 ethyl acetate/hexanes (0–100%) to provide the desired product as a yellow oil, 4.07 g (69%
9
10 yield). ¹H NMR (DMSO-d₆, 400 MHz) δ 7.98–7.64 (m, 3H), 7.64 (app d, *J* = 7.6, 1H), 4.38 (s,
11
12 2H), 3.82 (bs, 2H), 3.56 (t, *J* = 4.5 Hz, 1H), 2.36–1.98 (m, 3H), 1.82–1.70 (m, 6H), 1.15 (s, 9H),
13
14 1.14–1.07 (m, 4H). LC-MS *m/z* 509.2 (M+H); method A; RT = 2.42 min.

15
16
17
18
19
20 **4-((8-Azabicyclo[3.2.1]octan-3-yloxy)methyl)-5-cyclopropyl-3-(2-**
21
22 **(trifluoromethoxy)phenyl)isoxazole (1g).** *tert*-Butyl-3-((5-cyclopropyl-3-(2-
23 **(trifluoromethoxy)phenyl)isoxazol-4-yl)methoxy)-8-azabicyclo[3.2.1]octane-8-carboxylate (1f**
24
25 (3.98 g) was dissolved in a solution of 20% TFA in dichloromethane (30 mL). The solution was
26
27 stirred for 1 h at room temperature, and then the solvent was evaporated. The residue was
28
29 dissolved in ethyl acetate (125 mL) and washed with a saturated solution of sodium bicarbonate
30
31 (100 mL). The organic layer was dried with anhydrous sodium sulfate and evaporated *in vacuo*.
32
33 The crude residue was purified by silica gel chromatography using a gradient of 0–20%
34
35 ethanol/dichloromethane to afford 3.01 g of the desired product **1g** as a colorless oil (94% yield).
36
37 ¹H NMR (DMSO-d₆, 400 MHz) δ 8.51 (br s, 1H, NH), 7.72–7.68 (m, 1H), 7.64 (dd, *J* = 7.6,
38
39 1.8 Hz, 1H), 7.58–7.52 (m, 2H), 4.33 (s, 2H), 3.81 (bs, 2H), 3.55 (t, *J* = 4.5 Hz, 1H), 2.36–2.33
40
41 (m, 1H), 1.98 (app dt, *J* = 14.8, 4.0 Hz, 2H), 1.91–1.76 (m, 6H), 1.14–1.07 (m, 4H). LC-MS *m/z*
42
43 409.2 (M+H); method A; RT = 1.72 min.

44
45
46
47
48
49
50 **2-(3-((5-cyclopropyl-3-(2-(trifluoromethoxy)phenyl)isoxazol-4-yl)methoxy)-8-**
51
52 **azabicyclo[3.2.1]octan-8-yl)-4-fluorobenzo[d]thiazole-6-carboxylic acid (1).** Into a 25-mL
53
54 round-bottom flask equipped with a stir bar, the following were added sequentially: 4-((8-

1
2
3 azabicyclo[3.2.1]octan-3-yloxy)methyl)-5-cyclopropyl-3-(2-(trifluoromethoxy)phenyl)isoxazole
4
5 **1g** (0.525 g, 1.29 mmol), 3.6 mL of DMA, cesium carbonate (1.08 g, 3.31 mmol), and methyl 2-
6
7 chloro-4-methoxybenzo[d]thiazole-6-carboxylate **25a** (synthesis in the Supporting Information,
8
9 1.12 g, 3.87 mmol). After the resulting slurry was stirred at room temperature for 10 minutes,
10
11 the mixture was warmed to 60 °C and stirred for 1 h. The reaction was then allowed to cool to
12
13 room temperature, and it was diluted with 200 mL of ethyl acetate and washed with water (3×30
14
15 mL). The organic solvent extract was concentrated under vacuum and purified using by silica
16
17 gel chromatography (40 g silica column) with a gradient of ethyl acetate/hexanes (10–60%, 15
18
19 min gradient). Desired fractions were concentrated under vacuum, and the resulting residue
20
21 crystallized upon standing to furnish 0.60 g of desired intermediate methyl ester **1h** (75% yield).
22
23 ¹H NMR (DMSO_{d6}, 400 MHz) δ 8.13 (d, *J* = 1.6 Hz, 1H), 7.67–7.59 (m, 3H), 7.54–7.50 (m, 2H),
24
25 4.41 (s, 2H), 4.31 (bs, 2H), 3.90 (s, 3H), 3.60 (t, *J* = 4.8 Hz, 1H), 2.31–2.25 (m, 1H), 2.10 (app
26
27 dt, *J* = 14.8, 4.0 Hz, 2H), 2.02–1.91 (m, 4H), 1.83 (app d, *J* = 14.8 Hz, 2H), 1.19–1.15 (m, 4H).
28
29 LC-MS *m/z* 618.2 (M+H); method A; RT = 3.26 min. Into a 25-mL round-bottom flask
30
31 equipped with a stir bar was added sequentially: the methyl ester **1h** (0.55 g, 0.89 mmol), THF
32
33 (4.0 mL), MeOH (2.0 mL), and 3 N aqueous KOH solution (1 mL, 3 mmol). The resulting
34
35 homogenous solution was stirred for 1 h at 70 °C and then allowed to cool to room temperature.
36
37 The reaction was quenched with AcOH (0.2 mL of glacial acetic acid, 3 mmol) until pH=6 was
38
39 achieved as monitored by pH-strip paper (Whatman class type CF Cat. No 2613991). The
40
41 resulting solution was diluted with ethyl acetate (40 mL) and washed with water (3×5 mL). The
42
43 ethyl acetate layer was concentrated down to an oily residue via vacuum in a 40 mL Wheaton
44
45 glass vial, and this oil was then dissolved into MeOH (6 mL). The resulting homogenous
46
47 solution soon began to crystallize and allowed to stand for 2.5 h. The mother liquor was
48
49
50
51
52
53
54
55
56
57
58
59
60

1
2
3 withdrawn, and the crystals were washed with ice cold MeOH (3×2 mL). The crystals were dried
4
5 under vacuum (10 mm Hg pressure at 45 °C overnight). A first crop of crystals (516 mg, 91%
6
7 yield) were harvested and shown to be the methanol solvate by elemental analysis. Elemental
8
9 Analysis as the methanol solvate: (C₃₀H₂₉F₄N₃O₆S): C 56.69, H 4.60, N 6.61; Found: C 56.79, H
10
11 4.61, N 6.65. ¹H NMR (CDCl₃, 400 MHz, for the methanol solvate) δ (d, *J* = 2.0 Hz, 1H), 7.76
12
13 (dd, *J* = 9.0, 1.0 Hz, 1H), 7.57–7.50 (m, 2H), 7.43–7.36 (m, 2H), 4.37 (s, 2H), 4.35 (bs, 2H), 3.60
14
15 (t, *J* = 4.8 Hz, 1H), 3.50 (br s, 3H, peak corresponding to the presence of the methanol solvate),
16
17 2.19–2.10 (m, 3H), 2.03–1.90 (m, 4H), 1.83 (app d, *J* = 12.8 Hz, 2H), 1.22–1.19 (m, 2H), 1.15–
18
19 1.09 (m, 2H). LC-MS *m/z* 604.2 (M + 1).

20
21
22 The methanol solvate form of **1** was converted into a solvate-free crystalline form using the
23
24 following procedure: The methanol solvate of **1** (500 mg) was fully dissolved in dry acetonitrile
25
26 (50 mL) with gentle heating for 8 minutes (60 °C). This solution was allowed to stand for 4 days
27
28 to crystallize. Upon drying, 484 mg of crystals were obtained with two collection crops. High
29
30 Resolution Mass Spectroscopic analysis, 604.1514 for the [M+H]⁺ ion is consistent with the
31
32 molecular formula C₂₉ H₂₅ F₄ N₃O₅S, with a deviation of 1.6 ppm from the calculated [M+H]⁺
33
34 ion mass of 604.1530. Purity was found to be >99 % by LC-MS analysis, two separate protocols.
35
36 First protocol: [M+H]⁺ = 604.2 using LC-MS method A, RT = 3.22 min. Second LC-MS method
37
38 B, RT = 2.21 min, MS *m/z* 604.1 (M+H). IR (cm⁻¹): major stretches at 1679 (C=O stretch), 1242
39
40 (C-O-C stretch), 1213 (C-N stretch), 1167 (C-F stretch). Elemental Analysis of solvate free form
41
42 (C₂₉H₂₅F₄N₃O₅S): C 57.71, H 4.18, N 6.96; Found: C: 57.66, H: 4.20, N: 6.94. ¹H NMR
43
44 (DMSO-*d*₆, 400 MHz) δ 12.96 (br s, 1H), 8.20 (d, *J* = 1.5 Hz, 1H), 7.69–7.66 (m, 1H), 7.64 (dd, *J*
45
46 = 7.6, 1.7 Hz, 1H), 7.59–7.57 (m, 1H), 7.56–7.55 (m, 1H), 7.54 (d, *J* = 1.1 Hz, 1H), 4.34 (s, 2H),
47
48 4.22 (app d, *J* = 5.7 Hz, 2H), 3.55 (t, *J* = 4.7 Hz, 1H), 2.34 (tt, *J* = 8.39, 5.18, 1H), 2.01–1.95
49
50
51
52
53
54
55
56
57
58
59
60

1
2
3 (m, 2H), 1.86–1.82 (m, 4H), 1.75 (app d, $J = 14.5$ Hz, 2H), 1.16–1.13 (m, 2H), 1.10–1.07 (m,
4 2H). ^{19}F (DMSO- d_6 , 376 MHz) –126.4, –56.3 ppm. ^{13}C (DMSO- d_6 , 100 MHz) 171.79, 166.77,
5 166.37, 159.41, 151.70 (d, $J = 249$ Hz), 146.35, 145.10, 133.65 (d, $J = 5.2$ Hz), 132.26, 132.11,
6 128.25, 124.09, 123.22, 121.88, 120.40 (q, $J = 258.3$ Hz), 119.78, 113.39 (dd, $J = 19.2, 2.4$ Hz),
7 112.11, 72.35, 59.68, 57.28, 33.68, 27.91, 8.43, 7.50. M.P. = 221 °C sharp, corrected.
8
9
10
11
12
13
14
15
16
17
18
19
20
21
22
23
24
25
26
27
28
29
30
31
32
33
34
35
36
37
38
39
40
41
42
43
44
45
46
47
48
49
50
51
52
53
54
55
56
57
58
59
60

Assignment table for proton and carbon spectra is in the Supporting information.

ASSOCIATED CONTENT

Supporting Information

The Supporting Information is available free of charge on the ACS Publications website at
DOI:

Experimental procedures and analytical data for the synthesis of all compounds and Molecular
Formula Strings; FXR-HTRF coactivator interaction biochemical assay; FXR BSEP-luc reporter
gene cellular assay; rat in vitro hepatocyte gene expression assay; PK protocols; in vivo rat PD
study protocols. (PDF)

AUTHOR INFORMATION

Corresponding Author

*Tel: (510) 879-9456. E-mail: david.tully@novartis.com

Present Addresses

*(D.C.T) Novartis Institutes for Biomedical Research, Emeryville, California, USA

[†](A.P.) WuXi AppTec, San Francisco, California, USA

[‡](H.M.S.) IFM Therapeutics, Boston, Massachusetts, USA

§(S.B.J.) Calibr, La Jolla, California, USA

Notes

The authors declare no competing financial interest.

ACKNOWLEDGMENT

The authors thank David Jones for NMR assistance, Vivian Wang for technical assistance, Wendy Richmond and Perry Gordon for formulation support, Barbara Saechao for bioanalytical support, and Glen Spraggon for X-ray crystallography.

ABBREVIATIONS

FXR, Farnesoid X Receptor; NASH, nonalcoholic steatohepatitis; PBC, primary biliary cholangitis; PFIC, progressive familial intrahepatic cholestasis; BSEP, bile salt export pump; UDCA, ursodeoxycholic acid or ursodiol, SHP, short heterodimer partner; FGF15/FGF19, fibroblast growth factor 15/19; FGFR4; fibroblast growth factor receptor 4; LDL, low-density lipoprotein; MAPK, mitogen-activated protein kinase; CYP7A1, cytochrome P450 7A1 or cholesterol 7 α -hydroxylase, SREPB-1c, Sterol regulatory element-binding protein 1c; TGR5, G protein-coupled bile acid receptor 1 (GPBAR1); GPCR, G protein-coupled receptor; OCA, obeticholic acid; HTRF, Homogeneous Time Resolved Fluorescence; MDR3, multidrug resistance protein 3; ABCB4/ABCB11, ATP-binding cassette, sub-family B member 4/11; NR1H4, nuclear receptor subfamily 1, group H, member 4; SRC1, Steroid Receptor Coactivator-1, HLM, human liver microsomes; RLM, rat liver microsomes; FASSIF, fasted state simulated intestinal fluid; qPCR, quantitative polymerase chain reaction;

REFERENCES

- 1
2
3
4
5
6 (1) Chiang, J. Y. L. Bile Acids: Regulation of Synthesis. *J. Lipid Res.* **2009**, *50*, 1955–1966.
- 7
8 (2) Calkin, A. C.; Tontonoz, P. Transcriptional Integration of Metabolism by the Nuclear
9 Sterol-Activated Receptors LXR and FXR. *Nat. Rev. Mol. Cell Biol.* **2012**, *13*, 213–224.
- 10
11 (3) Goodwin, B.; Jones, S. A.; Price, R. R.; Watson, M. A.; McKee, D. D.; Moore, L. B.;
12 Galardi, C.; Wilson, J. G.; Lewis, M. C.; Roth, M. E. A Regulatory Cascade of the Nuclear
13 Receptors FXR, SHP-1, and LRH-1 Represses Bile Acid Biosynthesis. *Mol. cell* **2000**, *6*, 517–
14 526.
- 15
16 (4) Schaap, F. G.; Trauner, M.; Jansen, P. L. M. Bile Acid Receptors as Targets for Drug
17 Development. *Nat. Rev. Gastroenterol. & Hepatol.* **2013**, *11*, 55–67.
- 18
19 (5) Dyson, J. K.; Hirschfield, G. M.; Adams, D. H.; Beuers, U.; Mann, D. A.; Lindor, K. D.;
20 Jones, D. E. J. Novel Therapeutic Targets in Primary Biliary Cirrhosis. *Nat. Rev. Gastroenterol.*
21 *& Hepatol.* **2015**, *12*, 147–158.
- 22
23 (6) Srivastava, A. Progressive Familial Intrahepatic Cholestasis. *J. Clin. Exp. Hepatol.* **2014**,
24 *4*, 25–36.
- 25
26 (7) Chen, F.; Ananthanarayanan, M.; Emre, S.; Neimark, E.; Bull, L. N.; Knisely, A. S.;
27 Strautnieks, S. S.; Thompson, R. J.; Magid, M. S.; Gordon, R.; Balasubramanian, N.; Suchy, F.
28 J.; Shneider, B. L. Progressive Familial Intrahepatic Cholestasis, Type 1, Is Associated with
29 Decreased Farnesoid X Receptor Activity. *Gastroenterology* **2004**, *126*, 756–764.
- 30
31 (8) Gomez-Ospina, N.; Potter, C. J.; Xiao, R.; Manickam, K.; Kim, M.-S.; Kim, K. H.;
32 Shneider, B. L.; Picarsic, J. L.; Jacobson, T. A.; Zhang, J.; He, W.; Liu, P.; Knisely, A. S.;
33 Finegold, M. J.; Muzny, D. M.; Boerwinkle, E.; Lupski, J. R.; Plon, S. E.; Gibbs, R. A.; Eng, C.
34 M.; Yang, Y.; Washington, G. C.; Porteus, M. H.; Berquist, W. E.; Kambham, N.; Singh, R. J.;
- 35
36
37
38
39
40
41
42
43
44
45
46
47
48
49
50
51
52
53
54
55
56
57
58
59
60

1
2
3 Xia, F.; Enns, G. M.; Moore, D. D. Mutations in the Nuclear Bile Acid Receptor FXR Cause
4 Progressive Familial Intrahepatic Cholestasis. *Nat. Commun.* **2016**, *7*:10713. DOI:
5 10.1038/ncomms10713.
6
7
8

9
10 (9) Ali, A. H.; Carey, E. J.; Lindor, K. D. Recent Advances in the Development of Farnesoid
11 X Receptor Agonists. *Ann. Transl. Med.* **2015**, *3*(1):5. DOI: 10.3978/j.issn.2305-
12 5839.2014.12.06.
13
14
15

16
17 (10) Neuschwander-Tetri, B. A.; Loomba, R.; Sanyal, A. J.; Lavine, J. E.; Van Natta, M. L.;
18 Abdelmalek, M. F.; Chalasani, N.; Dasarathy, S.; Diehl, A. M.; Hameed, B.; Kowdley, K. V.;
19 McCullough, A.; Terrault, N.; Clark, J. M.; Tonascia, J.; Brunt, E. M.; Kleiner, D. E.; Doo, E.;
20 null, null. Farnesoid X Nuclear Receptor Ligand Obeticholic Acid for Non-Cirrhotic, Non-
21 Alcoholic Steatohepatitis (FLINT): A Multicenter, Randomized, Placebo-Controlled Trial.
22 *Lancet* **2015**, *385*.
23
24
25
26
27
28
29

30
31 (11) Hirschfield, G. M.; Mason, A.; Luketic, V.; Lindor, K.; Gordon, S. C.; Mayo, M.;
32 Kowdley, K. V.; Vincent, C.; Bodhenheimer, H. C.; Parés, A.; Trauner, M.; Marschall, H.-U.;
33 Adorini, L.; Sciacca, C.; Beecher-Jones, T.; Castelleo, E.; Böhm, O.; Shapiro, D. Efficacy of
34 Obeticholic Acid in Patients With Primary Biliary Cirrhosis and Inadequate Response to
35 Ursodeoxycholic Acid. *Gastroenterology* **2015**, *148*, 751–761.
36
37
38
39
40
41
42

43 (12) Bowlus, C. Obeticholic Acid for the Treatment of Primary Biliary Cholangitis in Adult
44 Patients: Clinical Utility and Patient Selection. *Hepatic Med. Evid. Res.* **2016**, *8*, 89–95.
45
46
47

48 (13) Pencek, R.; Marmon, T.; Roth, J. D.; Liberman, A.; Hooshmand-Rad, R.; Young, M. A.
49 Effects of Obeticholic Acid on Lipoprotein Metabolism in Healthy Volunteers. *Diabetes, Obes.*
50 *Metab.* **2016**, *18*, 936–940.
51
52
53
54

55 (14) A Multi-part, Double Blind Study to Assess Safety, Tolerability and Efficacy of LJN452
56
57
58
59
60

1
2
3 in PBC Patients. ClinicalTrials.gov Identifier: NCT02516605.

4
5 (15) Safety, Tolerability and Efficacy Study of 12 Weeks LJN452 Treatment in NASH
6
7 Patients (FLIGHT-FXR). ClinicalTrials.gov Identifier: NCT02855164.

8
9
10 (16) Maloney, P. R.; Parks, D. J.; Haffner, C. D.; Fivush, A. M.; Chandra, G.; Plunket, K. D.;
11
12 Creech, K. L.; Moore, L. B.; Wilson, J. G.; Lewis, M. C.; Jones, S. A.; Willson, T. M.
13
14 Identification of a Chemical Tool for the Orphan Nuclear Receptor FXR. *J. Med. Chem.* **2000**,
15
16 *43*, 2971–2974.

17
18
19 (17) Akwabi-Ameyaw, A.; Caravella, J. A.; Chen, L.; Creech, K. L.; Deaton, D. N.; Madauss,
20
21 K. P.; Marr, H. B.; Miller, A. B.; Navas, F.; Parks, D. J.; Spearing, P. K.; Todd, D.; Williams, S.
22
23 P.; Wisely, G. B. Conformationally Constrained Farnesoid X Receptor (FXR) Agonists:
24
25 Alternative Replacements of the Stilbene. *Bioorganic & Med. Chem. Lett.* **2011**, *21*, 6154–6160.

26
27 (18) Bass, J. Y.; Caravella, J. A.; Chen, L.; Creech, K. L.; Deaton, D. N.; Madauss, K. P.;
28
29 Marr, H. B.; McFadyen, R. B.; Miller, A. B.; Mills, W. Y.; Navas III, F.; Parks, D. J.; Smalley
30
31 Jr., T. L.; Spearing, P. K.; Todd, D.; Williams, S. P.; Wisely, G. B. Conformationally
32
33 Constrained Farnesoid X Receptor (FXR) Agonists: Heteroaryl Replacements of the
34
35 Naphthalene. *Bioorganic & Med. Chem. Lett.* **2011**, *21*, 1206–1213.

36
37 (19) Smalley Jr., T. L.; Boggs, S.; Caravella, J. A.; Chen, L.; Creech, K. L.; Deaton, D. N.;
38
39 Kaldor, I.; Parks, D. J. Novel Heterocyclic Scaffolds of GW4064 as Farnesoid X Receptor
40
41 Agonists. *Bioorganic & Med. Chem. Lett.* **2015**, *25*, 280–284.

42
43 (20) Bass, J. Y.; Caldwell, R. D.; Caravella, J. A.; Chen, L.; Creech, K. L.; Deaton, D. N.;
44
45 Madauss, K. P.; Marr, H. B.; McFadyen, R. B.; Miller, A. B.; Parks, D. J.; Todd, D.; Williams,
46
47 S. P.; Wisely, G. B. Substituted Isoxazole Analogs of Farnesoid X Receptor (FXR) Agonist
48
49 GW4064. *Bioorganic & Med. Chem. Lett.* **2009**, *19*, 2969–2973.
50
51
52
53
54
55
56
57
58
59
60

- 1
2
3 (21) Akwabi-Ameyaw, A.; Bass, J. Y.; Caldwell, R. D.; Caravella, J. A.; Chen, L.; Creech, K.
4
5 L.; Deaton, D. N.; Jones, S. A.; Kaldor, I.; Liu, Y.; Madauss, K. P.; Marr, H. B.; McFadyen, R.
6
7 B.; Miller, A. B.; Navas III, F.; Parks, D. J.; Spearing, P. K.; Todd, D.; Williams, S. P.; Wisely,
8
9 G. B. Conformationally Constrained Farnesoid X Receptor (FXR) Agonists: Naphthoic Acid-
10
11 Based Analogs of GW 4064. *Bioorganic & Med. Chem. Lett.* **2008**, *18*, 4339–4343.
12
13
14 (22) Abel, U.; Schlüter, T.; Schulz, A.; Hambruch, E.; Steeneck, C.; Hornberger, M.;
15
16 Hoffmann, T.; Perović-Ottstadt, S.; Kinzel, O.; Burnet, M.; Deuschle, U.; Kremoser, C.
17
18 Synthesis and Pharmacological Validation of a Novel Series of Non-Steroidal FXR Agonists.
19
20 *Bioorganic & Med. Chem. Lett.* **2010**, *20*, 4911–4917.
21
22
23 (23) Gege, C.; Kinzel, O.; Steeneck, C.; Kremoser, A. S. and C. Knocking on FXR's
24
25 Door: The “Hammerhead”-Structure Series of FXRs Agonists - Amphiphilic Isoxazoles with
26
27 Potent In Vitro and In Vivo Activities. *Curr. Top. Med. Chem.* **2014**, *14*, 2143–2158.
28
29
30 (24) Xu, Y. Recent Progress on Bile Acid Receptor Modulators for Treatment of Metabolic
31
32 Diseases. *J. Med. Chem.* **2016**, *59*, 6553–6579.
33
34
35 (25) Genin, M. J.; Bueno, A. B.; Agejas Francisco, J.; Manninen, P. R.; Bocchinfuso, W. P.;
36
37 Montrose-Rafizadeh, C.; Cannady, E. A.; Jones, T. M.; Stille, J. R.; Raddad, E.; Reidy, C.; Cox,
38
39 A.; Michael, M. D.; Michael, L. F. Discovery of 6-(4-([5-Cyclopropyl-3-(2,6-
40
41 Dichlorophenyl)isoxazol-4-Yl]methoxy)piperidin-1-Yl)-1-Methyl-1H-Indole-3-Carboxylic
42
43 Acid: A Novel FXR Agonist for the Treatment of Dyslipidemia. *J. Med. Chem.* **2015**, *58*, 9768–
44
45 9772.
46
47
48 (26) Tully, D. C.; Vidal, A.; Mutnick, D.; Alper, P. B. Compositions and Methods for
49
50 Modulating Farnesoid X Receptors. WO 2012/087520 A1, June 28, 2012.
51
52
53 (27) Tully, D. C.; Rucker, P. V.; Alper, P. B.; Mutnick, D.; Chianelli, D. Compositions and
54
55
56
57
58
59
60

1
2
3 Methods for Modulating FXR. WO 2012/087519 A1, June 28, 2012.

4
5 (28) Alemi, F.; Kwon, E.; Poole, D. P.; Lieu, T.; Lyo, V.; Cattaruzza, F.; Cevikbas, F.;
6
7 Steinhoff, M.; Nassini, R.; Materazzi, S.; Guerrero-Alba, R.; Valdez-Morales, E.; Cottrell, G. S.;
8
9 Schoonjans, K.; Geppetti, P.; Vanner, S. J.; Bunnett, N. W.; Corvera, C. U. The TGR5 Receptor
10
11 Mediates Bile Acid-induced Itch and Analgesia. *J. Clin. Investig.* **2013**, *123*, 1513–1530.
12
13

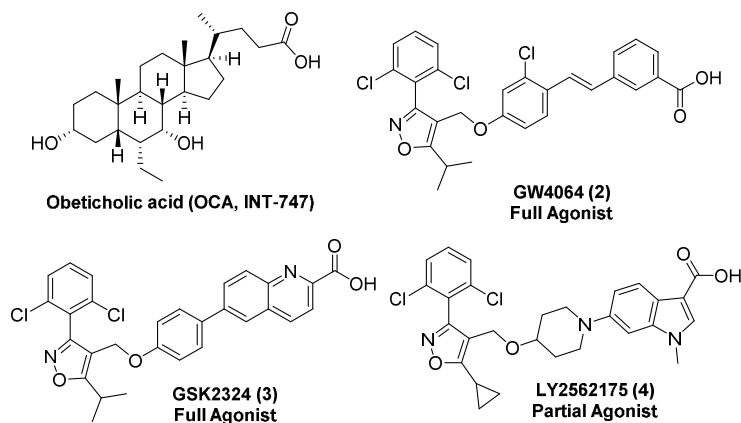
14
15 (29) Lieu, T.; Jayaweera, G.; Zhao, P.; Poole, D. P.; Jensen, D.; Grace, M.; McIntyre, P.;
16
17 Bron, R.; Wilson, Y. M.; Krappitz, M.; Haerteis, S.; Korbmacher, C.; Steinhoff, M. S.; Nassini,
18
19 R.; Materazzi, S.; Geppetti, P.; Corvera, C. U.; Bunnett, N. W. The Bile Acid Receptor TGR5
20
21 Activates the TRPA1 Channel to Induce Itch in Mice. *Gastroenterology* **2014**, *147*, 1417–1428.
22
23

24
25 (30) Nevens, F.; Andreone, P.; Mazzella, G.; Strasser, S. I.; Bowlus, C.; Invernizzi, P.;
26
27 Drenth, J. P. H.; Pockros, P. J.; Regula, J.; Beuers, U.; Trauner, M.; Jones, D. E.; Floreani, A.;
28
29 Hohenester, S.; Luketic, V.; Shiffman, M.; Erpecum, K. J. van; Vargas, V.; Vincent, C.;
30
31 Hirschfield, G. M.; Shah, H.; Hansen, B.; Lindor, K. D.; Marschall, H.-U.; Kowdley, K. V.;
32
33 Hooshmand-Rad, R.; Marmon, T.; Sheeron, S.; Pencek, R.; MacConell, L.; Pruzanski, M.;
34
35 Shapiro, D. A Placebo-Controlled Trial of Obeticholic Acid in Primary Biliary Cholangitis. *New*
36
37 *Engl. J. Med.* **2016**, *375*, 631–643.
38
39

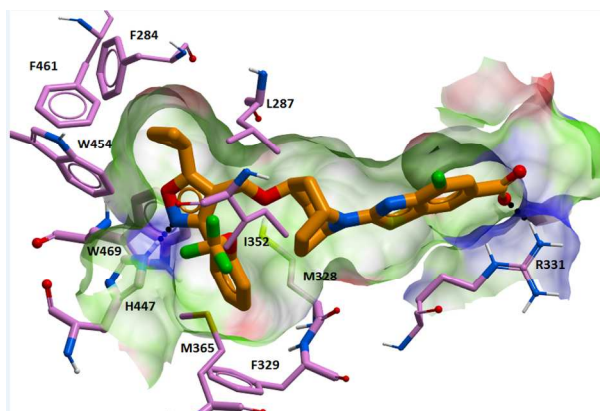
40
41 (31) US FDA: Ocaliva Full Prescribing Information (US Package Insert for Commercial Use),
42
43 2017.
44

45
46 (32) (a) Badman, M. K.; Desai, S.; Laffitte, B.; Decristofaro, M.; Lin, T.; Chen, J.; Reilly, J. F.;
47
48 Klickstein, L. First-in-Human experience with LJN452, an orally available non-bile acid FXR
49
50 agonist, demonstrates potent activation of FXR in healthy subjects. AASLD Abstracts, The
51
52 Liver Meeting, Boston, MA, Nov 11–15, 2016; *Hepatology*, October **2016**, *64*:1, 32. (b) Laffitte,
53
54 B.; Hernandez, E. D.; Zheng, L.; Kim, Y.; Liu, B.; Valdez, R. A.; Dietrich, W. F.; Rucker, P.;
55
56
57
58
59
60

1
2
3 Chianelli, D.; Schmeits, J.; Bao, D.; Zoll, J.; Chen, L.; Joseph, S. B.; Klickstein, L. B.; Chen, J.;
4
5
6 Xu, J.; Tully, D. C.; Molteni, V.; McNamara, P.; Badman, M. K. Tropifexor (LJN452) Improves
7
8 Cholestasis, Steatohepatitis and Hepatic Fibrosis in Rodents without Altering Plasma Lipids in
9
10 Humans. *Submitted*.



31 **Figure 1.** Examples of FXR agonists reported in the literature.



48 **Figure 2.** Model of **1** docked into FXR ligand binding domain, from X-ray structure of PDB
49 code: 3DCT.

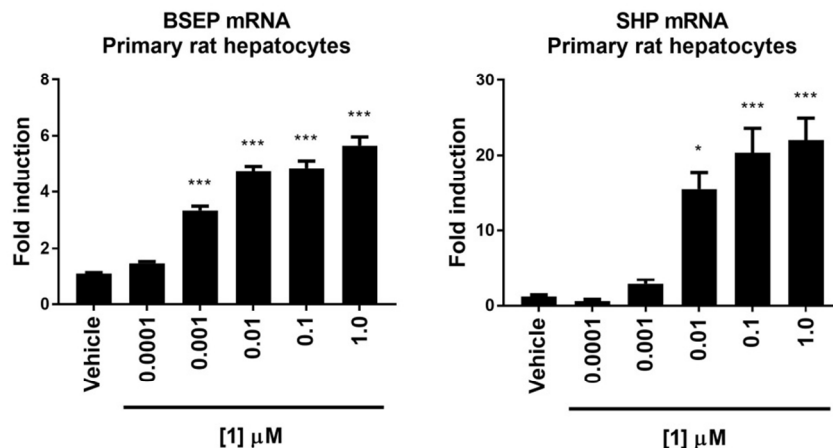


Figure 3. Induction of FXR target genes BSEP and SHP in vitro in rat primary hepatocytes by compound **1**. Primary rat hepatocytes were treated for 24 h with compound **1** or vehicle only, and gene expression was determined by real-time quantitative PCR. * $p \leq 0.01$, ** $p \leq 0.001$, and *** $p \leq 0.0001$ compared to vehicle by one-way ANOVA.

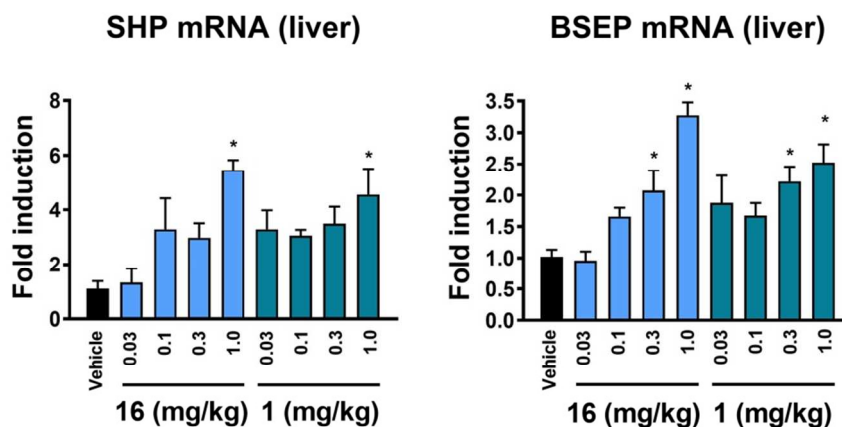


Figure 4. Induction of FXR target genes SHP and BSEP in rat liver by compounds **1** and **16** following single oral dose. Dose in mg/kg; vehicle 0.5% methylcellulose, 0.5% Tween80, 99% water, suspension. * $p \leq 0.01$ versus vehicle by one-way ANOVA.

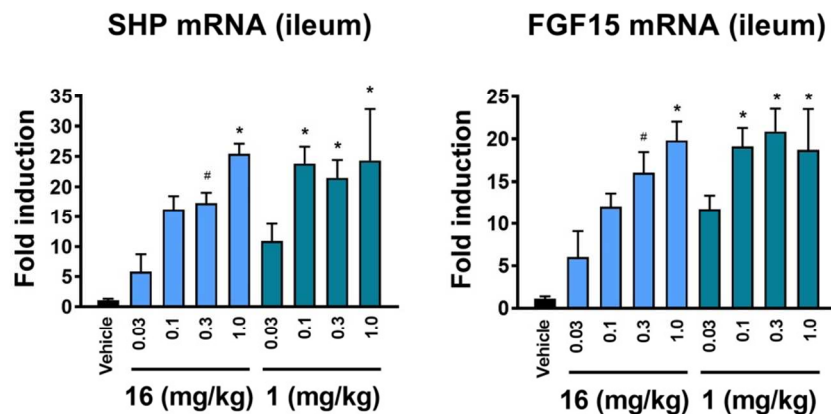


Figure 5. Induction of FXR target genes SHP and FGF15 in rat ileum by compounds **1** and **16** following single oral dose. Dose in mg/kg; vehicle 0.5% methylcellulose, 0.5% Tween80, 99% water, suspension. # $p \leq 0.05$ and * $p \leq 0.01$ vs. vehicle by one-way ANOVA.

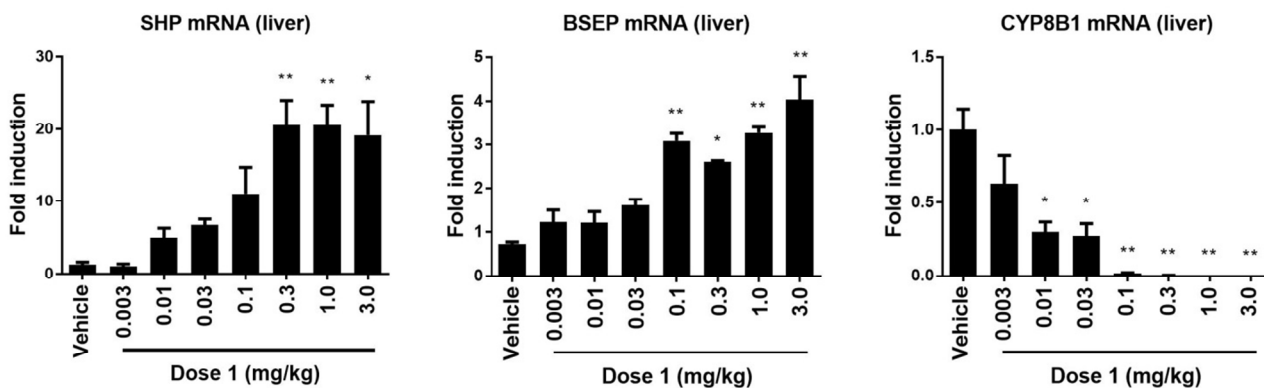


Figure 6. Induction of FXR target genes SHP, BSEP, and CYP8B1 in rat liver following oral administration of compound **1** once daily for 14 days. Dose in mg/kg; vehicle 0.5% methylcellulose, 0.5% Tween80, 99% water, suspension. * $p \leq 0.01$ and ** $p \leq 0.001$ versus vehicle by one-way ANOVA.

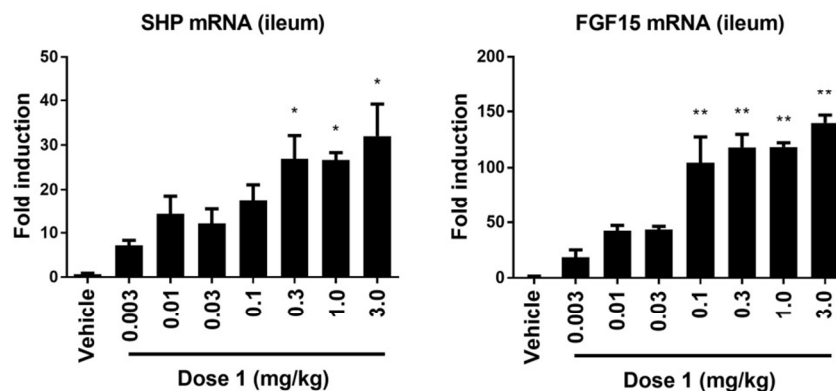


Figure 7. Induction of FXR target genes SHP and FGF15 in rat liver following oral administration of compound **1** once daily for 14 days. Dose in mg/kg; vehicle 0.5% methylcellulose, 0.5% Tween80, 99% water, suspension. * $p \leq 0.01$ and ** $p \leq 0.001$ versus vehicle by one-way ANOVA.

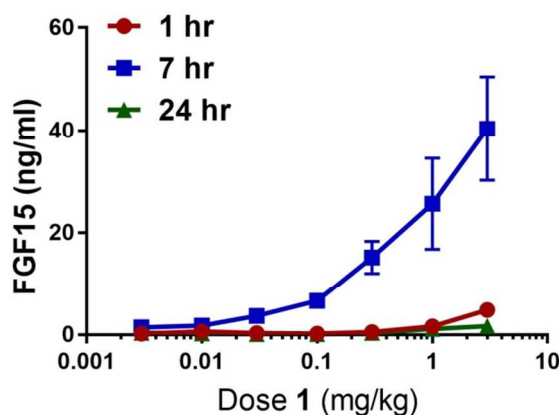


Figure 8. Plasma FGF15 levels on day 14, at 1 h, 7 h, and 24 h following oral administration of compound **1** once daily for 14 days. Dose in mg/kg; vehicle 0.5% methylcellulose, 0.5% Tween80, 99% water, suspension.

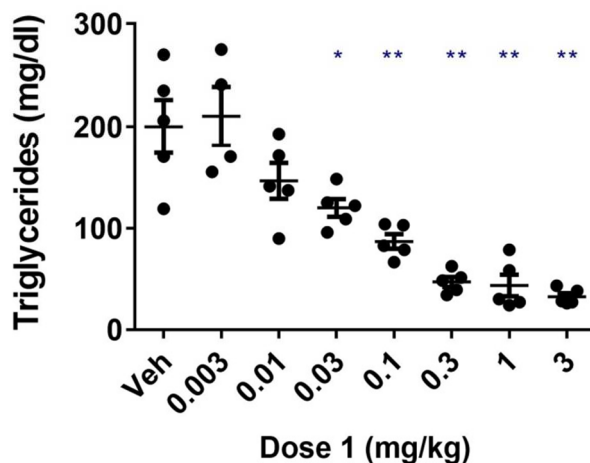


Figure 9. Serum triglycerides on day 15, at 24h following oral administration of compound **1** once daily for 14 days. Dose in mg/kg; vehicle 0.5% methylcellulose, 0.5% Tween80, 99% water, suspension. * $p \leq 0.01$ and ** $p \leq 0.001$ versus vehicle by one-way ANOVA.

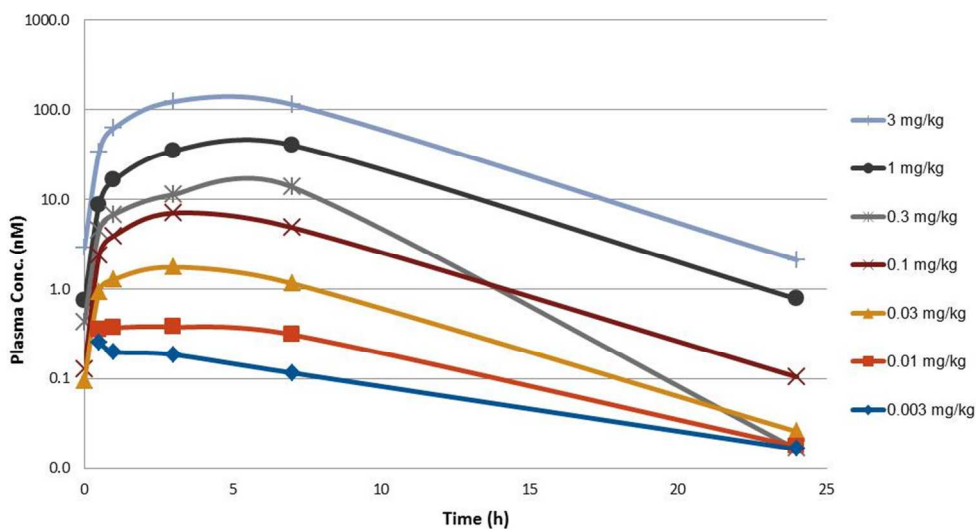
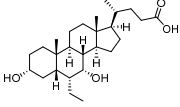
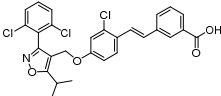
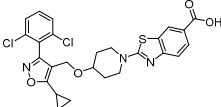
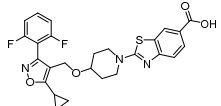
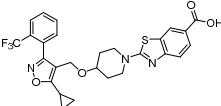
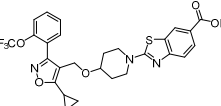
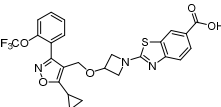
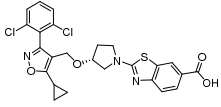
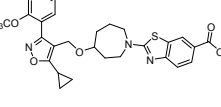
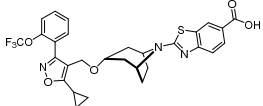


Figure 10. Steady state pharmacokinetics (day 11) of compound **1**; mean total plasma concentration versus time profiles ($n = 3$).

Table 1. Optimization of phenyl substituent and linker.^a

Entry	Structure	cLogD	FXR HTRF EC ₅₀ (nM) (% efficacy)	FXR BSEP- Luciferase EC ₅₀ (nM) (% efficacy)	Solubility pH=6.8 FASSIF (μM)	Metabolic stability RLM, HLM (ER)
OCA		2.8	10 (96)	42 (63)	–	–
2		5.4	19 (100)	95 (100)	–	–
5		3.2	8.3 (96)	9.5 (118)	61	0.58, 0.81
6		2.2	31 (84)	88 (92)	169	0.52, 0.27
7		2.9	66 (97)	70 (103)	131	0.50, 0.38
8		3.1	19 (97)	19 (100)	70	<0.18, <0.21
9		2.1	1580 (69)	8400 (63)	–	–
10		2.8	3060 (47)	9200 (46)	–	–
11		3.5	4.2 (120)	6.6 (108)	126	0.75, 0.89

12		3.40	0.54 (93)	0.69 (89)	110	0.51, <0.20
----	---	------	-----------	-----------	-----	-------------

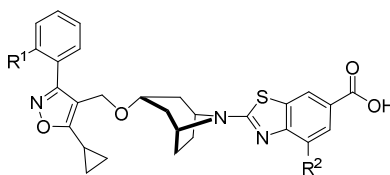
^aValues are the mean of three or more experiments

Table 2. Rat PK data of selected FXR agonists.

Compound d	Intravenous ^a			Oral Administration ^b		
	CL (mL/min/ kg)	V _{ss} (L/kg)	T _{1/2} (h)	AUC (h*nM)	C _{max} (nM)	F (%)
5	50	0.55	0.34	390	44	6
8	24	1.2	1.0	4571	382	37
12	17	1.1	1.0	1923	173	11
13	14	0.84	1.0	832	86	3
14	9	0.26	0.7	2670	1988	9
1	9	0.72	3.7	6042	2279	20
15	11	0.70	3.7	3446	2121	14
16	11	0.60	1.8	3636	2108	14

^a(3 mg/kg) 75%PEG300:25%D5W, solution; ^b(10 mg/kg) solution vehicle: 75% PEG300:25% D5W (compounds **5**, **8**, **12**, **13**) or microemulsion vehicle: water (90%), cremophor RH40 (4.5%), corn oil (1.8%), PEG400 (2.7%), ethanol (1%), (compounds **1**, **14**, **15**, **16**).

Table 3. Optimization of benzothiazole substituent.^a



Entry	R ¹	R ²	cLogD	pKa (carboxylic acid)	FXR HTRF EC ₅₀ (nM) (% efficacy)	FXR BSEP- Luciferase EC ₅₀ (nM) (% efficacy)	Solubility pH=6.8 FASSIF (μM)	Metabolic stability RLM, HLM (ER)
12	-OCF ₃	-H	3.40	5.1	0.54 (93)	0.69 (89)	110	0.51, <0.20
13	-OCF ₃	-Me	3.9	5.5	0.49 (91)	0.82 (79)	< 10	<0.18, <0.21
14	-OCF ₃	-OMe	3.4	4.5	0.57 (78)	0.42 (89)	75	0.50, 0.64
1	-OCF ₃	F	3.5	4.0	0.20 (92)	0.26 (89)	600	<0.18, 0.55
15	-OCHF ₂	F	2.7	4.0	0.27 (92)	0.80 (87)	750	0.40, 0.61
16	-CF ₃	F	3.3	4.0	0.46 (90)	0.54 (77)	510	0.19, 0.36

^aValues are the mean of three or more experiments

Table 4. Mean ED₅₀ at 7 h for selected FXR target genes in liver and ileum following oral administration of compound **1** once daily for 14 days.

Gene (mRNA)	ED ₅₀ at 7h (mg/kg)	CV (%)
Liver SHP	0.02	28.9
Liver BSEP	0.02	34.6

Liver CYP8B1	0.01	64.0
Ileum SHP	0.01	75.8
Ileum FGF15	0.05	32.8

Table 5. Steady state pharmacokinetics (days 1 and 11) of compound **1**; mean C_{max} and AUC(0-24h) (n = 3).

Dose (mg/kg)	Day	C_{max} (nM)	AUC(0-24hr) nM*hr	AUC(0-24h) / Dose	Accumulation AUC day 11 / day1
0.003	1	0.15	2	668	
	11	0.26	2	756	1.1
0.01	1	0.44	4	443	
	11	0.79	5	496	1.1
0.03	1	1.5	15	503	
	11	1.9	20	658	1.3
0.1	1	4.6	41	410	
	11	7.1	80	796	1.9
0.3	1	13.5	117	390	
	11	14.8	190	633	1.6
1	1	39.3	461	461	
	11	43.1	562	562	1.2
3	1	171.8	1344	448	
	11	127.1	1688	563	1.3

Table 6. Mean plasma and liver concentrations of compound **1** at steady state, 1 h and 7 h post-dose, following oral administration once daily for 14 days.

Dose (mg/kg)	Time (h)	Tissue	Mean Conc. (nM)	SD (nM)	Ratio Liver/Plasma
0.003	1	plasma	0.20	0.10	15
		liver	2.92	0.35	
	7	plasma	0.12	0.06	20
		liver	2.30	0.66	
0.01	1	plasma	0.37	0.15	22
		liver	8.35	0.51	
	7	plasma	0.31	0.07	17
		liver	5.18	0.71	
0.03	1	plasma	1.29	0.21	9
		liver	11.86	3.35	
	7	plasma	1.16	0.49	8
		liver	9.74	1.26	
0.1	1	plasma	3.95	1.17	7
		liver	27.35	10.48	
	7	plasma	4.89	1.01	9
		liver	44.98	9.67	
0.3	1	plasma	6.84	0.34	12
		liver	84.46	3.64	
	7	plasma	13.78	1.52	7
		liver	92.78	6.91	
1.0	1	plasma	16.41	2.16	10
		liver	159.11	45.58	
	7	plasma	40.54	18.31	6
		liver	229.84	44.40	
3.0	1	plasma	62.61	1.97	14
		liver	872.12	405.26	
	7	plasma	114.72	17.88	6
		liver	639.75	235.68	

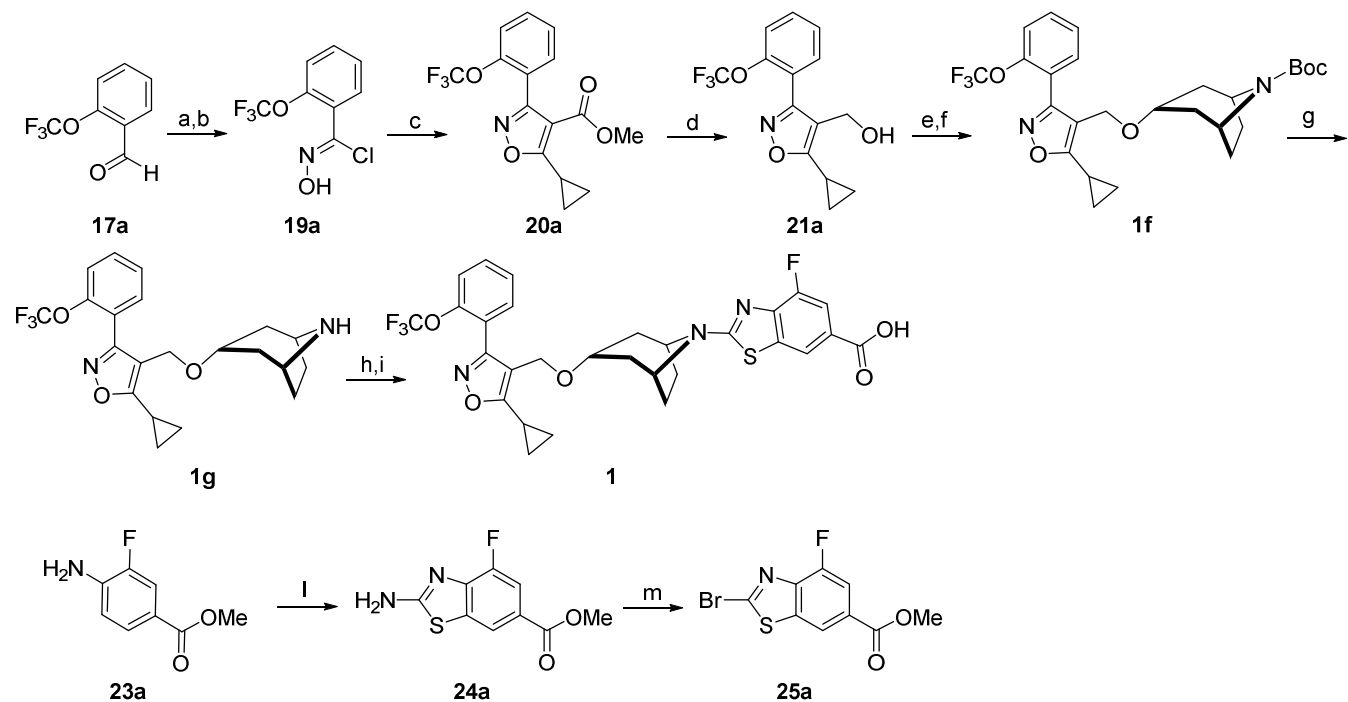
Table 7. TGR5 agonist activities of compound **1**, OCA, and OCA conjugates.

Compound	hTGR5	mTGR5
	EC ₅₀ (μM)	EC ₅₀ (μM)
	(% vs control)	(% vs control)
1	> 10	> 10
OCA	0.918 (83%)	5.74 (68%)
OCA-aurine conjugate	0.205 (102%)	0.906 (97%)
OCA-glycine conjugate	0.315 (101%)	0.637 (98%)

Table 8. PK profile of **1** across multiple species.

Property	Mouse	Rat	Dog
Dose	IV = 5	IV = 3	IV = 0.5
(mg/kg)	PO = 10	PO = 1	PO = 2
IV CL	5.3	9.3	1.5
(mL/min/kg)			
V _{ss} (L/kg)	0.70	0.72	0.46
IV T _{1/2} (h)	2.6	3.7	7.4
Oral AUC	4785	307	3660
(h*nM)			
Oral C _{max}	1186	53	332
(nM)			
Oral F (%)	9.2	10	10
PPB	~99.9	~99.9	~99.9
(% Bound)			

^aIV (3 mg/kg) 75% PEG300:25% D5W, solution (mouse and rat); 20% PEG300, 5% Solutol, 75% carbonate buffer pH=8, solution (dog); PO Vehicle 0.5% methylcellulose, 0.5% Tween80, 99% water, suspension (mouse, rat and dog)



Scheme 1. Synthesis of compound **1**, reagents and conditions. a) $NH_2OH \cdot HCl$, H_2O , 10 min, 0 °C, 83%; b) NCS, DMF, 1 h, 25 °C, 99%; c) K_2CO_3 , methyl 3-cyclopropyl-3-oxopropanoate, THF, -5 °C to 35 °C, 52%; d) $LiAlH_4$, THF, -10 °C, 30 min, 93%; e) CBr_4 , PPh_3 , THF, 1h, rt, 87%; f) N-Boc nortropine, 18-crown-6, THF, potassium *tert*-butoxide, 18 h, rt, 69%; g) TFA, DCM, 1h, rt, 94%; h) **25a**, Cs_2CO_3 , DMA, 1 h, rt to 60 °C, 75%; i) KOH, MeOH, THF, 1 h, 70 °C, 91%; l) NaSCN, AcOH, Br_2 , 0 °C to 30 °C over 48 h 66%; m) $CuBr_2$, MeCN, *t*-BuONO, 0 °C to 30 °C, 48h, 24%.

1
2
3
4
5
6
7
8
9
10
11
12
13
14
15
16
17
18
19
20
21
22
23
24
25
26
27
28
29
30
31
32
33
34
35
36
37
38
39
40
41
42
43
44
45
46
47
48
49
50
51
52
53
54
55
56
57
58
59
60

Insert Table of Contents artwork here

